Journal of Magnetic Resonance 208 (2011) 148–155

Contents lists available at ScienceDirect

Journal of Magnetic Resonance

journal homepage: www.elsevier.com/locate/jmr

Finite element analysis of gradient *z*-coil induced eddy currents in a permanent MRI magnet

Xia Li [a], Ling Xia [a,*], Wufan Chen [b], Feng Liu [c], Stuart Crozier [c], Dexin Xie [d]

[a] Department of Biomedical Engineering, Zhejiang University, Hangzhou 310027, China
[b] Department of Biomedical Engineering, Southern Medical University, Guangzhou 510515, China
[c] School of Information Technology & Electrical Engineering, University of Queensland, St. Lucia, Brisbane, Queensland 4072, Australia
[d] School of Electrical Engineering, Shenyang University of Technology, Shenyang 111078, China

ARTICLE INFO

Article history:
Received 12 April 2010
Revised 28 October 2010
Available online 4 November 2010

Keywords:
Permanent magnet MRI
Eddy currents
Finite element analysis
Ferromagnetic materials
Preisach model

ABSTRACT

In permanent magnetic resonance imaging (MRI) systems, pulsed gradient fields induce strong eddy currents in the conducting structures of the magnet body. The gradient field for image encoding is perturbed by these eddy currents leading to MR image distortions. This paper presents a comprehensive finite element (FE) analysis of the eddy current generation in the magnet conductors. In the proposed FE model, the hysteretic characteristics of ferromagnetic materials are considered and a scalar Preisach hysteresis model is employed. The developed FE model was applied to study gradient *z*-coil induced eddy currents in a 0.5 T permanent MRI device. The simulation results demonstrate that the approach could be effectively used to investigate eddy current problems involving ferromagnetic materials. With the knowledge gained from this eddy current model, our next step is to design a passive magnet structure and active gradient coils to reduce the eddy current effects.

1. Introduction

In MRI, the patient is placed in a strong, static magnetic field in which the hydrogen nuclei within the human body resonate at a radio-frequency (RF) (Larmor frequency) that is proportional to the static field strength. Transmission and reception coils operating at the Larmor radio-frequency are placed near and around the patient to excite and receive the MR signals from the hydrogen nuclei. These signals are spatially encoded by gradient coils and digitally processed to form MR images. Magnet and gradient coils are therefore critical field generating devices in MRI.

The permanent magnet (PM) type of MRI system had been developed because of their advantages of small leakage flux and low operating cost [1–6]. In a whole-body PM MRI systems, the magnets are assembled with ferromagnetic materials, such as pole pieces and the yoke. The gradient coils are generally located close to the magnet poles and include three independent coils that produce gradients in the main field along the three Cartesian axes (i.e. *x*-, *y*- and *z*-coils). During MRI operation, gradient coils are amplitude modulated with a trapezoidal or sinusoidal waveform, with a usual gradient rise time of several hundred microseconds. The pulsed gradient currents will induce strong eddy currents in surrounding conducting structures. The magnetic fields caused by these eddy currents will distort the linear gradient fields produced by the gradient coils and therefore deteriorate the spatial location of signal from the sample.

Since the early development of the MRI technology, numerical modeling has been a useful tool for the analysis of eddy currents problems in an effort to provide solutions for the minimization of their effects on MR images. For example, finite-difference time-domain (FDTD) models [7,8] and numerical hybrid models (FE method and integration method) [9,10] have been developed for the analysis of eddy currents in the superconducting MRI systems. Compared with superconducting MRI systems, the eddy currents problems in permanent MRI systems are more complicated, this is because the pole pieces and the yoke are made of soft ferromagnetic materials, which have nonlinear and hysteretic properties; that is, the permeability or reluctivity of the materials vary with both time and location. Each alternate pulse current will make the operating point of *B*–*H* curve of ferromagnetic materials move on the minor local loop. Numerical methods [7–10] for superconducting magnet structures are not straightforwardly applicable to the transient magnetic diffusion through the ferromagnetic materials. Therefore a dynamic analysis of hysteresis of ferromagnetic materials in a PM MRI system is essential for the characterization of the transient eddy current effects and for the effective compensation/control and further advancement of the imaging system. To model the loop effects, Miyata et al. [11,12] and Takahashi et al. [13–15] have simulated the magnetic field at a low field (0.12 T) PM assembly consisting

* Corresponding author. Fax: +86 571 87951676.
E-mail address: xialing@zju.edu.cn (L. Xia).

1090-7807/$ - see front matter © 2010 Elsevier Inc. All rights reserved.
doi:10.1016/j.jmr.2010.10.017

of four columns. While the piecewise linear method can sometimes be used to model the hysteresis loop in a steady-state situation, it is not flexible enough to be used as a generalized dynamic modeling method [16].

'High field' (say ~0.5 T or above) PM assemblies for MRI systems have been developed in recent years. Compared to the low-field PM MRI device, the residual magnetization of magnets in a high field PM MRI magnet system is higher, and there exists more saturated states in the ferromagnetic elements. Moreover, to further enhance the strength and uniformity of the main magnetic field, extra PM material is employed and directions of residual magnetization are position dependent. These issues require more complicated mathematical/physical models to enable accurate calculations. There is a lack of depth of investigations on the establishment of eddy current models for high field PM MRI systems. In this work, we will construct an FE model for eddy currents modeling of a high field PM system.

Under periodic excitation conditions, the magnetic flux density B of ferromagnetic material is not a single-valued function of magnetic field strength H, but is related to the history of magnetism state. There are many approaches to describe the hysteresis characteristics used in industrial applications, in which the classical Preisach model is especially practical for hysteresis modeling [17]. This model has been refined for the ease of tracing the magnetism and identifying the instantaneous B–H operating point of nonlinear system and the combination of FEM and Preisach model has previously been used in the eddy currents analyses for electrical machine [16,18–22]. Recently, this model has also been used for the study of characteristics of permanent magnet materials [23]. The FE method has proven to be an effective numerical technique to solve electromagnetic field problems, including model large-scale eddy current problems in electromagnetic engineering [24–29]. In this paper, the eddy currents in pole pieces are analyzed using the FE method combined with a scalar Preisach model.

2. Methods

2.1. Model of PM MRI scanner

The electromagnetic system of a PM MRI device includes the permanent magnet and conducting materials, such as pole pieces, yoke and pluggings, plugging rings, and gradient coils. Fig. 1 shows the cross-section of a C-type PM assembly for an MRI device with vertical static magnetic flux density of 0.5 T, and for the gradient z-coil, the homogeneous region of the gradient linearity is a diameter sphere volume (DSV) of 40 cm. The yoke is made of steel (steel-1010), the conductivity of which is 2×10^6 S/m. The pole piece and plugging ring are made of electrically pure iron (DT4) whose conductivity is 1.03×10^7 S/m. The NdFeB permanent magnet, the source of main magnetic field, has a coercivity of 1,034,507 A/m and a relative permeability of 1.0439. The plugging is also made of NdFeB whose coercivity is 940,045 A/m and relative permeability is 1.038. The gradient z-coils having 16 turns (shown in Fig. 2) are located near the surface of the pole piece to generate a longitudinal gradient field which is excited by a pulse current (see Fig. 3) and the switching rate of the coils is 0.125 mT/m/A. The pulse sequence is repeated and only one cycle including ten trapezoid pulses has been shown in Fig. 3b. In the model, the cross-section of each current-carrying loop is 6(width) × 3(thick) mm^2. The gradient rise time is 500 μs and each pulse is divided into 100 steps. The time step Δt is small enough to pick up any rapid temporal change in the source of field. In order to reduce the CPU time and memory requirement, the 3D model has been simplified to a 2D model to enable calculation based on the axisymmetric of z gradient coils.

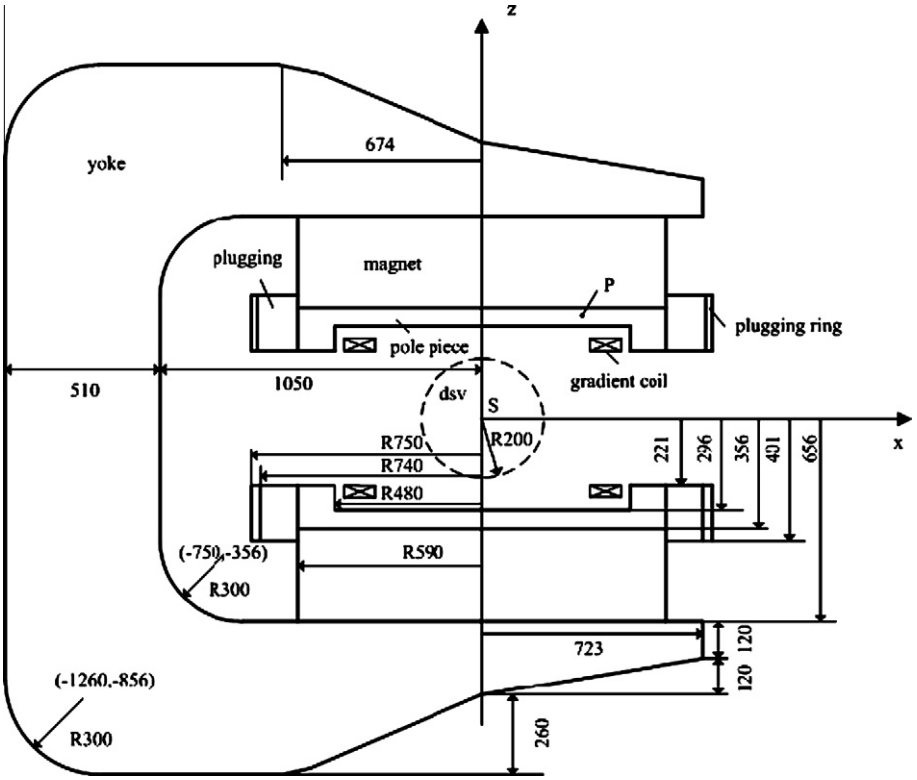

Fig. 1. Cross-section of permanent magnet assembly. Magnets are used to generate main magnetic field, the pluggings are used to change the direction of magnetic field and enhance the main magnetic field intensity. There exits a special boundary between two PM materials. The spatial dimensions of the magnet structures have also been shown in millimeters.

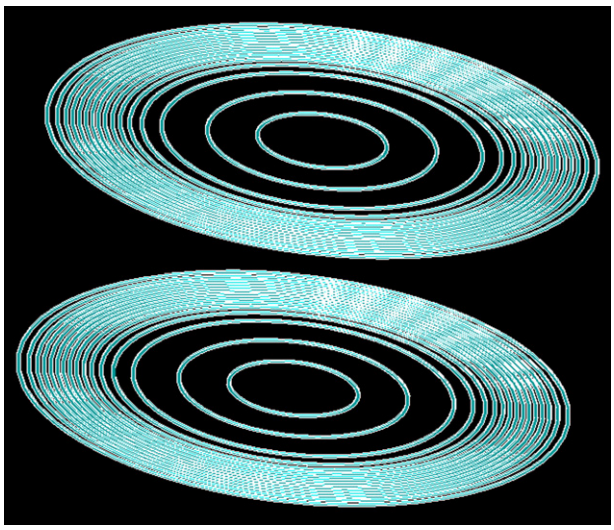

Fig. 2. Structure of gradient coils for analysis, the cross-section of each current-carrying loop is 6(width) × 3(thick) mm^2. The coils are located on the plane of $z = \pm 221$ mm and the radius of each loop in unit millimeter is 106, 188, 263, 295, 315, 331, 344, 356, 367, 377, 387, 398, 409, 420, 434 and 451, respectively.

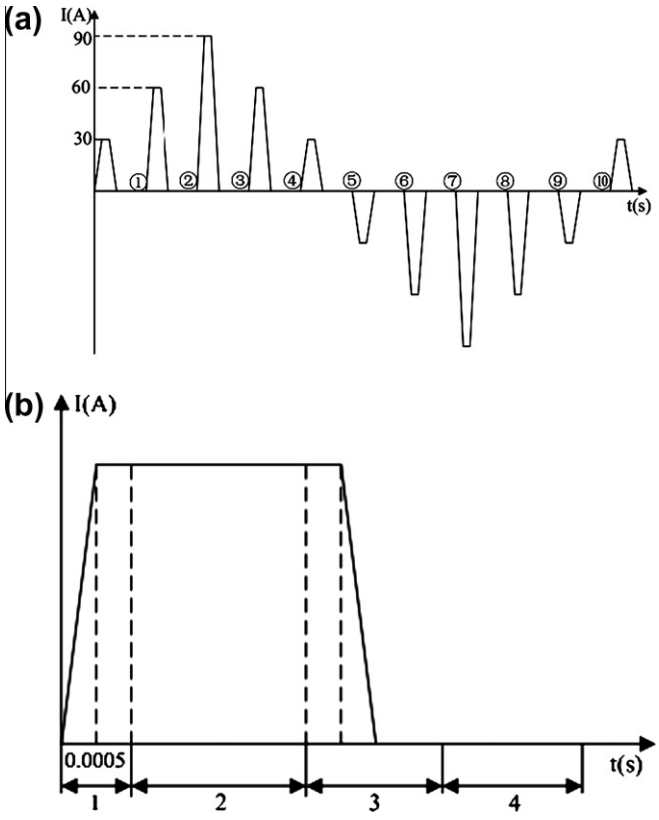

Fig. 3. Pulse current in the z gradient coils. (a) Pulse series, one cycle concludes ten trapezoid pulses. In order to demonstrate the phenomenon of hysteresis and eddy currents effects, the gradient waveform with a large number of zero-current states is purposely used for this investigation. (b) Enlarged pulse. The time (marked as number of steps times the time interval) for four periods is $20 \times 5 \times 10^{-5}$ s, $10 \times 4 \times 10^{-4}$ s, $40 \times 5 \times 10^{-5}$ s and 30×0.01 s, respectively.

2.2. Numerical method

2.2.1. Governing equations

The gradient–magnet interactions are governed by the following equations:

$$\begin{cases} \Delta \times (v\Delta \times A) + \sigma \frac{\partial A}{\partial t} = J_s \\ v_1 \frac{\partial A}{\partial t}|_{L^+} - v_2 \frac{\partial A}{\partial n}|_{L^-} = J_m \end{cases} \tag{1}$$

where A is the magnetic vector potential, J_s is the current density vector in the gradient coils, v is the reluctivity, σ is the conductivity, J_m is the equivalent magnetizing current density on the line L, the border of the NdFeB materials and other materials, which is parallel to the direction of the residual magnetization of the permanent magnet (shown in Fig. 4), and

$$J_m = \frac{B_r}{\mu_0} = \mu_r H_c \tag{2}$$

In which, B_r is the residual magnetization of PM, μ_0, is the permeability of vacuum, μ_r, H_c denote the relative permeability and the coercivity of NdFeB materials, respectively.

Applying the well-known Galerkin FE method [30], a differential matrix equation can be obtained as follows:

$$[K][A] + [D][\dot{A}] = [f] \tag{3}$$

where $\dot{A}$ denotes the time derivative of A, K and D are the coefficients matrix, f is the active source vector.

Meshing the domain with triangles, if one numbers the nodes in counterclockwise manner (see numerals i, j and m in Fig. 5), then the immediate parameters $b_i^e, b_j^e, b_m^e, c_i^e, c_j^e, c_m^e$ can be defined for the nodes (i, j, m), as expressed in the following equation:

$$\begin{cases} b_i^e = z_j^e - z_m^e & c_i^e = x_m^e - x_j^e \\ b_j^e = z_m^e - z_i^e & c_j^e = x_i^e - x_m^e \\ b_m^e = z_i^e - z_j^e & c_m^e = x_j^e - x_i^e \end{cases} \tag{4}$$

where $x_h^e, z_h^e (h = i, j, m)$ denotes the coordinates of the hth node in the given element.

Then for element e,

$$\begin{cases} K_{ij}^e = \frac{v}{4\Delta^e}(b_i^e b_j^e + c_i^e c_j^e) \\ D_{ij}^e = \sigma \frac{\Delta^e}{12}(1 + \delta_{ij}) \quad \delta_{ij} = \begin{cases} 1 & i = j \\ 0 & i \neq j \end{cases} \\ f_l^e = \frac{J_s \Delta^e}{3} \quad (l = i, j, m) \end{cases} \tag{5}$$

where Δ^e is the area of element e.

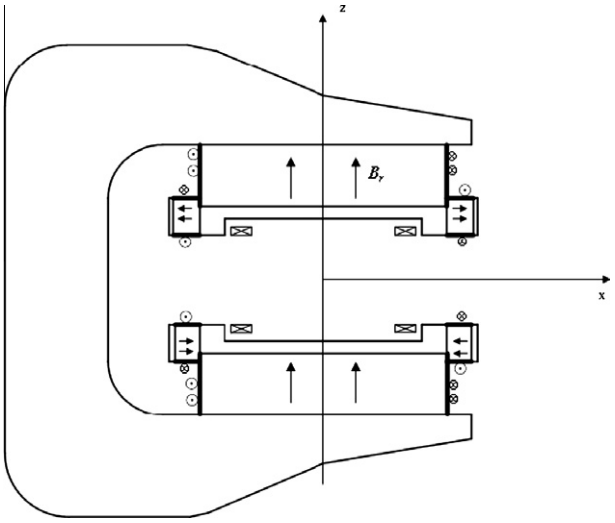

Fig. 4. The equivalent magnetizing current densities of the NdFeB materials. The locations of the equivalent magnetizing current densities are denoted in thick lines and the directions are also shown. The arrows show the directions of the residual magnetization of NdFeB materials in the magnets and the pluggings.

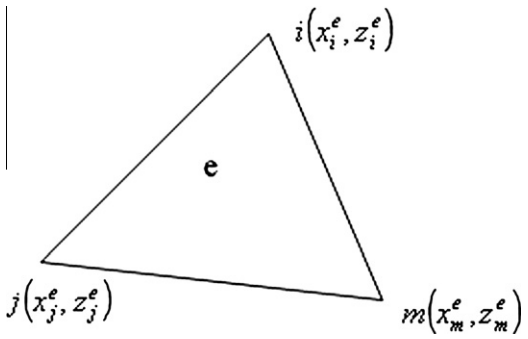

Fig. 5. Illustration of the finite element e in the model.

If j, m are on the boundary L, then:

$$\begin{cases} f_i^e = \frac{J_s \Delta^e}{3} \\ f_j^e = \frac{J_s \Delta^e}{3} + \frac{J_m S_i}{2} \\ f_m^e = \frac{J_s \Delta^e}{3} + \frac{J_m S_i}{2} \end{cases} \tag{6}$$

where S_i is the length of the line j_m.

Using a time-stepping method and backward difference method, we have:

$$\left[\frac{\partial A}{\partial t}\right]^{t+\Delta t} = \frac{[A]^{t+\Delta t} - [A]^t}{\Delta t} \tag{7}$$

Eq. (3) is then expressed as:

$$\left([K]^{t+\Delta t} + \frac{1}{\Delta t}[D]\right)[A]^{t+\Delta t} = [f]^{t+\Delta t} + \frac{1}{\Delta t}[D][A]^t \tag{8}$$

2.2.2. Hysteresis model

During gradient switching, the operating point on the B–H curve of the ferromagnetic material will move on the limiting loops or on the local hysteresis loops (as shown in Fig. 6). The magnetization curve has n local extrema, that is, reversal points. The magnetic flux density on a downward trajectory and upward trajectory can be calculated by the refined scalar Preisach model proposed by Hui and Zhu [16], respectively, that is on downward trajectory:

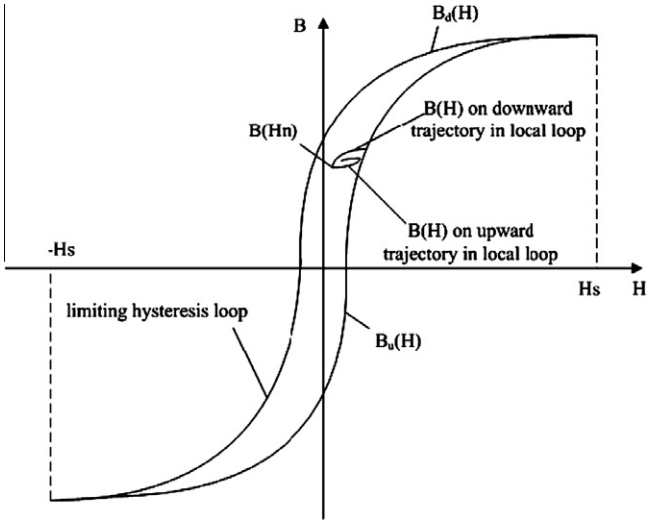

Fig. 6. Local minor loop and limiting hysteresis loops of ferromagnetic material. The limiting hysteresis loop is symmetrical about the base point of the coordinate axis.

$$B(H) = B(H_n) - 2T(H_n, H) \tag{9}$$

and on upward trajectory

$$B(H) = B(H_n) + 2T(H, H_n) \tag{10}$$

where H_n is the magnetic intensity of nth reversal point. The function $T(\alpha, \beta)$ is given as:

$$T(\alpha, \beta) = \frac{B_u(\alpha) - B_d(\beta)}{2} + F(\alpha)F(-\beta) \tag{11}$$

In which, the function $F(\alpha)$ is expressed as

$$F(\alpha) = \frac{B_d(\alpha) - B_u(-\alpha)}{2\sqrt{B_d(\alpha)}} \quad (\alpha \geqslant 0) \tag{12}$$

and

$$F(\alpha) = \sqrt{B_d(-\alpha)} \quad (\alpha < 0) \tag{13}$$

where $-H_s \leqslant \beta \leqslant \alpha \leqslant H_s$, H_s is the saturation magnetic field strength, α and β are the threshold values of magnetic intensity on the Preisach magnetic dipoles, B_u and B_d, the only predefined data in Preisach model, are the values of the magnetic flux density on the up and down trajectory of limiting hysteresis loop, respectively.On the initial magnetization curve, the magnetic flux density B_i is written as:

$$B_i(H) = [F(-H) - F(H)]^2 \tag{14}$$

Initially, the operating point of B–H curve moves on the initial magnetization curve; at each transient time step, magnetic field strength H is iteratively given by

$$H_{k+1} = H_k + \omega(H'_k - H_k) \tag{15}$$

where k denotes the kth iteration, H'_k is the magnetic intensity acquired from Preisach model, ω is the relaxation factor ($0 < \omega < 1$) and 0.5 is used in this case. The criterion of convergence is given as:

$$\frac{\sum_{e=1}^{NE} \left| H_{k+1}^{(e)} - H_k^{(e)} \right|}{\sum_{e=1}^{NE} \left| H_{k+1}^{(e)} \right|} < \varepsilon \tag{16}$$

where e is element number and NE is the total number of elements, and ε is the specified tolerance.

2.2.3. Preisach model implementation

The Preisach model can be easily implemented and the flow chart of the modeling process has been illustrated in Fig. 7.

A stack is designed to keep the B,H values of each reversal point. Before the simulation starts, the stack is initialized to zero. The stack content is updated according to the current H field value: If the H value decreases, the large value in the stack will be replaced by the current H value; if the H value increases, the small value in the stack will be replaced by the current H value. The temporal reversal points will be eliminated from a completed minor loop, since they will not have any effect on the future state of magnetization [16].

3. Results

3.1. Main magnetic flux lines and gradient magnetic flux lines

Fig. 8a shows the distribution of main magnetic flux lines produced by permanent magnet. It is noted that the z component of magnetic flux density (B_z) at the DSV is about 0.50 T. Fig. 8b illustrates the equi-potential lines of the gradient magnetic field at the transient 211th time step (any time point can be selected except the zero current time point. In order to illustrate the variation of

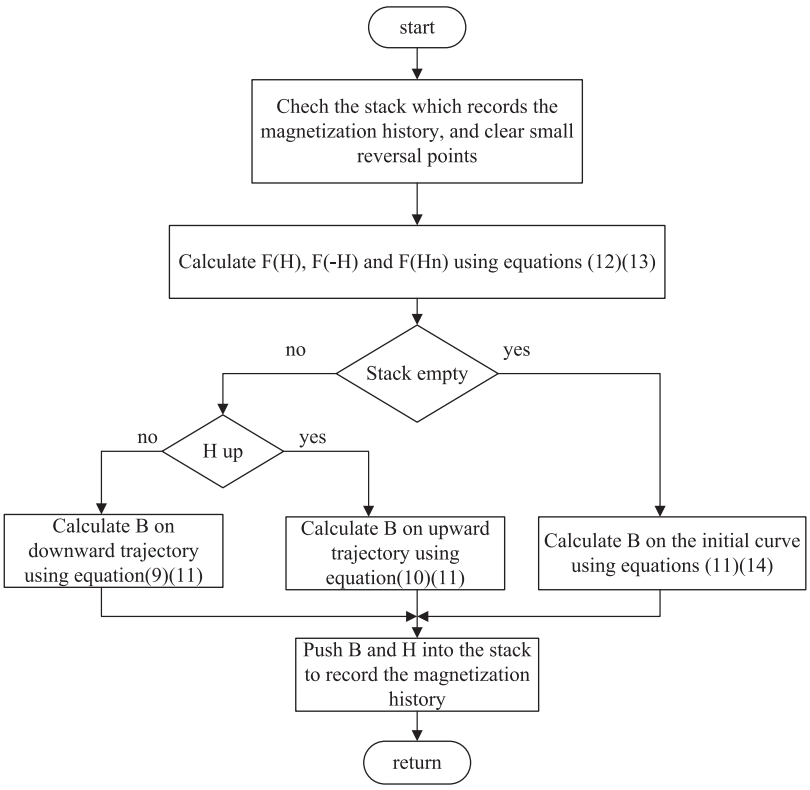

Fig. 7. Flow chart of the Preisach model.

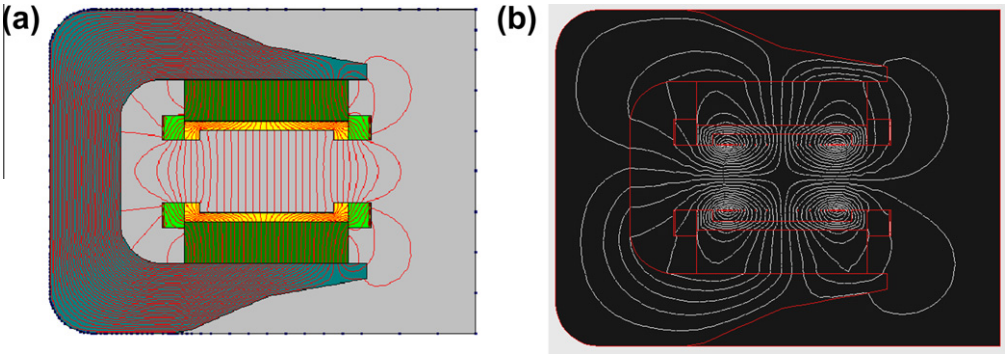

Fig. 8. Magnetic flux lines of the main magnetic field and equi-potential lines of gradient magnetic field. (a) Main magnetic field generated by PM materials. (b) Field produced only by gradient currents at the 211th time step. The pole pieces and plugging rings are near to the gradient coils and a higher magnetic flux density will be generated under a relatively low external magnetic field in electrically pure iron, so only the hysteresis of pole pieces and plugging rings are taking into account in the process.

the magnetic field clearly, the 211th time step is selected). It can be seen the gradient currents mainly electromagnetically affect the pole pieces, and therefore the hysteresis in the yoke is not considered in this work.

3.2. Magnetic flux density in DSV

Fig. 9 shows the time variation of the original field and the secondary fields B_z at the sampling point $S(x = 0, z = 0)$, which is the isocentre of the DSV. To illustrate the variation of the magnetic field due to eddy current distortions, we considered those time points without zero-currents, such as the time step 211th, which is close to the situation that the current reaches its maximum. The abscissa denotes the time step. It is clear that eddy currents have decreased the flux density, and more importantly, the time that the magnetic intensity reaches the maximum has been delayed, so the desired fast rise of the gradient magnetic field will be slowed.

Fig. 10 compared the ideal (a) and real (b) gradient field distribution in the DSV (an area of $0.4 \times 0.4\ m^2$ is shown) at the 211th time step. It is seen that the proposed model can clearly predict that eddy currents damage the linearity of gradient field in the imaging region.

3.3. Residual flux density

ΔB The change of residual magnetic flux intensity ΔB at point $P(x = 0.30\ m, z = 0.25\ m)$ in the pole piece labeled in Fig. 1 is calculated and shown in Fig. 11 (a). The definition of ΔB is given as

$$\Delta B = B_{z_k} - B_{z0P} \tag{17}$$

where B_{z_k} is the z component of the flux density at the instant ①, ②,..., when the current becomes zero after the impression of the

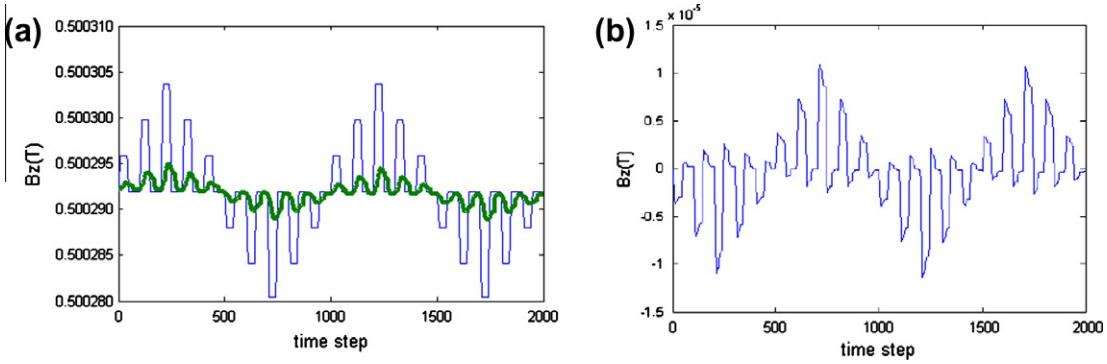

Fig. 9. Change of magnetic flux density with time (point *S* in DSV). (a) The thin line indicates the instantaneous original field without considering eddy currents, the broad line indicates the temporal magnetic flux intensity with eddy currents. (b) Secondary magnetic flux density generated by eddy currents with time. It is shown that the secondary field is opposite to the original field and suppresses the change of gradient field.

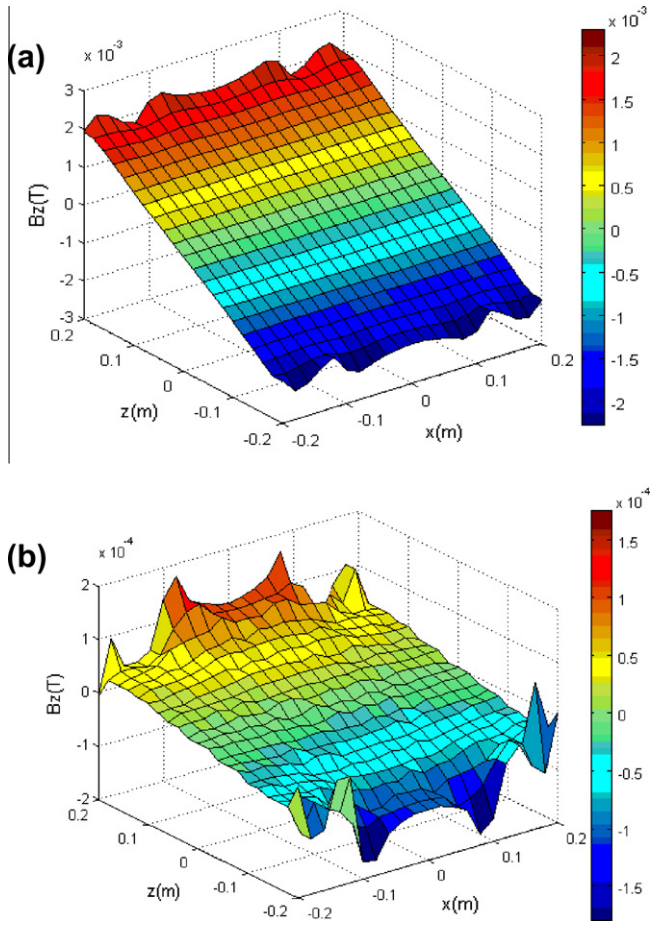

Fig. 10. The B_z distribution in the DSV. (a) The field of B_z generated by gradient currents without considering the eddy currents and a good linearity is shown in the DSV. (b) The field of B_z with eddy currents. It is shown that the eddy currents degrade the amplitude of the field and destroy the gradient magnetic intensity.

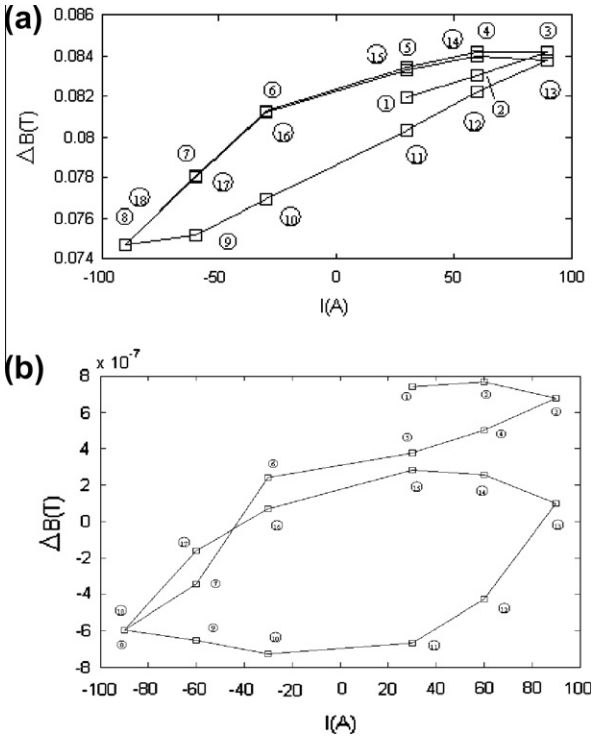

Fig. 11. Change of residual flux density ΔB. (a) At the point *P* in the pole piece. (b) At the point *S* in the DSV. The abscissa denotes the input currents of gradient pulse, and the field changes including eddy current effects at the time after the gradient transition are calculated. The circled numbers in this figure correspond to the timing of the circled numbers shown in Fig. 4.

*k*th pulse current (shown in Fig. 3), B_{zOP} is the *z* component of the flux density of point *P* at the instant $t = 0$ ($I = 0$ A). Obviously, ΔB is always equal to zero if there is no eddy current and no hysteresis.

The phenomenon of residual magnetic fields in the DSV is similar to that in the pole pieces, and the ΔB at point *S* in the DSV (labeled in Fig. 1) is shown in Fig. 11b. From Fig. 9, it can be seen that ΔB does not reach steady state until the eighteen pulses (about two periods) due to eddy currents and hysteresis.

4. Discussion

In high field PM MRI devices, the nonlinearity and hysteresis of the soft ferromagnetic materials are larger than the lower field cases, therefore the eddy currents problems are more complicated. Based on the Preisach hysteresis model, our FE model can analyze the large nonlinear eddy current problem of C-type PM MRI assembly with the inclusion of minor loops of soft ferromagnetic materials. With this model, the behavior of residual magnetic fields, in the pole pieces, caused by the hysteresis characteristics of ferromagnetic materials has been investigated. The actual gradient fields in PM MRI systems are influenced by the eddy currents and also the hysteresis characteristics of ferromagnetic materials. This information will be valuable for the design of compensation boards

for eddy currents in high field PM MRI systems. The passive shield board is usually made of silicon steel sheet, which has high, anisotropic permeability and resistance. The FEM model was developed for the analysis of laminated structure. The thickness of the eddy current board was determined by the consideration of the shielding effect and also practical space limits, and then verified using FE analysis. A fully automatic FEM-based optimization procedure is not used in this study due to high computational cost. We suggest that the optimal solution for eddy current management in permanent MRI system will be the combined technique, that is active shielding and passive shielding.

4.1. Advantages of the Preisach model

In previous similar work [9–12], the upper part of minor loop is modeled using the measured several hysteresis curves of ferromagnetic materials and which is approximated by a cubic spline function. System errors will occur due to a linear interpolation approximation. Furthermore, the lower part of the minor loop is mirrored from the upper part with a symmetry assumption. The error introduced from this approximation is negligible only if the amplitude of the minor loop is small enough. The preisach method does need to use linear interpolation to obtain B_u and B_d and this will introduce interpolation errors. But these errors are much smaller compared to previous models, which require several measured hysteresis curves and interpolations, usually involving large measurement and interpolation assumption errors [14]. In the Preisach model, the model data required is only for the limiting B–H loop, in which the measurement error is relatively small [16]. Comparatively, the Preisach model is more accurate, more flexible to identify the B–H operating point of the nonlinear materials and can be implemented straightforwardly within the FEM framework.

4.2. FE mesh grid

Mesh grid quality is very important for FEM analysis. To properly model eddy currents, the permanent magnet materials must be modeled with fine mesh structures, because rough mesh structures will introduce large computational errors in modeling of the minor loop. Fig. 12 demonstrates the employed mesh grid and Table 1 shows the discretization data and CPU time in the calculating process. As expected, the calculation time in the case of eddy currents is much more than that without considering the eddy currents. It is noted that for the current 2D FE analysis, the calculation time is mainly determined by the nonlinear iteration of permeability instead of the mesh size. However, for the full 3D analysis, the mesh size will significantly influence the solution and the selection of which will be a trade-off between accuracy and computational cost.

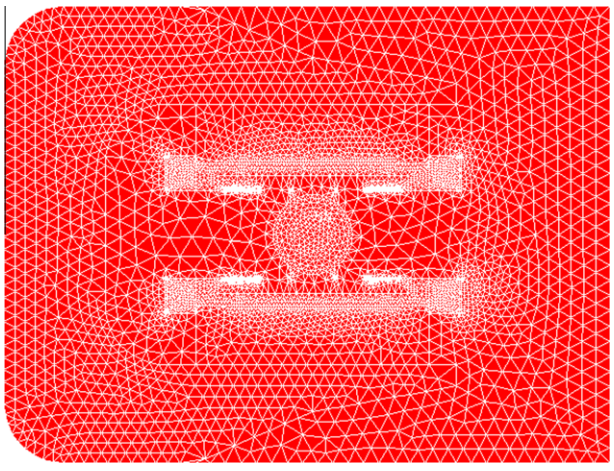

Fig. 12. Mesh grid of the solved region. The yoke is not a closed magnetic circuit and the right part of the magnet body is open to the air, so the air in the vicinity of right part of magnet body is included to analyze the eddy current problem.

Table 1
Discretization data and CPU time (on a computer with: inter(R) core(TM)2 quad CPU Q6600 at 2.40 GHz).

	Without eddy current	With eddy current
Number of elements	11,573	
Number of nodes	5863	
Number of time steps	1000	3501
CPU time (h)	0.4	6.0

4.3. Time interval Δt

The interval Δt is also an important parameter for the calculation of nonlinear eddy currents. When Δt is too large, the change of instantaneous fields will not be reflected during gradient switching. Initially, the time interval is determined in the light of that in reference [11], then adjusted with the investigated magnetic field variations. In this work, in the rapid changing portions around gradient transitions, a small time interval is employed, while in slower transition periods a larger time interval is used. Other advanced temporal discretization schemes, such as the Newmark-beta method (http://en.wikipedia.org/wiki/Newmark-beta-method), can be used to improve the numerical performance of the proposed FE model.

4.4. Residual flux density ΔB

The major cause for the residual flux density is the hysteresis characteristics of the ferromagnetic pole pieces and the variation of ΔB is nonlinearly following the slow-decaying eddy currents, for the worst case shown here, it took about 18 pulses to reach steady state. In practical cases, the steady state can be reached earlier due to non-perfect conducting environment. The change of ΔB is larger when eddy currents become larger.

5. Conclusion

In this paper, an FE analysis of nonlinear eddy current problems for a 0.5 T permanent magnet-type MRI system has been presented. Based on the Preisach model, the hysteretic characteristics of soft ferromagnetic materials have been taken into account, and it has been shown that the change of residual flux intensity occurs because of the minor loop of electrically pure iron. The transient, eddy current distorted gradient field can be effectively modeled. With this model available, it is possible to optimally design novel eddy current compensation shields using laminated structures (such as anisotropic Fe–Si) and to improve the gradient coil design so as to minimize eddy current generation.

Acknowledgments

This project is supported by the 973 National Basic Research & Development Program (2010CB732502) of China, China Postdoctoral Science Foundation (20090451468) and National Nature Science Funds of China (30900332).

References

[1] S. Masato, S. Fujimura, Y. Matsuura, Magnetic Materials and Permanent Magnets, US Patent No. 4770723, 1998.

[2] A. Momy, J. Taquin, Low-leakage wide-access magnet for MRI, IEEE Trans. Magn. 33 (1997) 4572–4574.
[3] B. Manz, M. Benecke, F. Volke, A simple small and low cost permanent magnet design to produce homogeneous magnetic fields, J. Magn. Reson. 192 (2008) 131–138.
[4] C. Bauer, H. Raichv, G. Jeschke, P. Blumler, Design of a permanent magnet with a mechanical sweep suitable for variable-temperature continuous-wave and pulsed EPR spectroscopy, J. Magn. Reson. 198 (2009) 222–227.
[5] K. Hirokazu, K. Kanji, T. Norio, et al., A design of permanent magnet array for unilateral NMR device, Concept Magn. Reson. B 33 (2008) 201–208.
[6] M. Giorgio, M. Richard, Miniature permanent magnet for table-top NMR, Concept Magn. Reson. B 19 (2003) 35–43.
[7] F. Liu, S. Crozier, An FDTD model for calculation of gradient-induced eddy currents in MRI system, IEEE Trans. Appl. Supercond. 14 (2004) 1983–1989.
[8] A. Trakic, H. Wang, F. Liu, L.H. Sanchez, S. Crozier, Analysis of transient eddy currents in MRI using a cylindrical FDTD method, IEEE Trans. Appl. Supercond. 16 (2006) 1924–1936.
[9] T. Takahashi, Numerical analysis of eddy current problems involving *z* gradient coils in superconducting MRI magnets, IEEE Trans. Magn. 26 (1990) 893–896.
[10] T. Takahashi, Numerical analysis of eddy current problems involving saddle-shaped coils in superconducting MRI magnets, IEEE Trans. Magn. 27 (1991) 3996–3999.
[11] K. Miyata, K. Ohashi, N. Takahashi, H. Ukita, Analysis of magnetic characteristics of permanent magnet assembly for MRI devices taking account of hysteresis and eddy current, IEEE Trans. Magn. 34 (1998) 3556–3559.
[12] K. Miyata, K. Ohashi, A. Muraoka, N. Takahashi, 3-D magnetic field analysis of permanent-magnet type of MRI taking account of minor loop, IEEE Trans. Magn. 42 (2006) 1451–1454.
[13] N. Takahashi, K. Miyata, T. Kayamo, K. Ohashi, Effect of minor loop on magnetic characteristics of permanent magnet type of MRI, IEEE Trans. Magn. 35 (1999) 1893–1896.
[14] N. Takahashi, K. Miyata, R. Suenage, K. Ohashi, Analysis of the magnetic property of a permanent-magnet-type MRI-behavior of residual magnetization, IEEE Trans. Magn. 39 (2003) 1337–1340.
[15] T. Takahashi, A. Muraoka, D. Miyagi, K. Miyata, K. Ohashi, 3-D FEM analysis of residual magnetism produced by *x*-gradient coil of permanent magnet type of MRI, IEEE Trans. Magn. 43 (2007) 1809–1812.
[16] S.Y.R. Hui, J. Zhu, Numerical modeling and simulation of hysteresis effects in magnetic cores using transmission-line modeling and the Preisach theory, IEE Proc. Electr. Power Appl. 142 (1995) 57–62.
[17] F. Preisach, Uber die magnetische Nachwirkung Zeit, Physik 94 (1935) 277–302.
[18] P. Alotto, P. Girdinio, P. Molfino, A 2D finite element procedure for magnetic analysis involving non-linear and hysteretic materials, IEEE Trans. Magn. 30 (1994) 3379–3382.
[19] J.H. Lee, J.C. Kim, D.S. Hyun, Effect analysis of magnet on Ld and Lq inductance of permanent magnet assisted synchronous reluctance motor using finite element method, IEEE Trans. Magn. 35 (1999) 1199–1202.
[20] J.H. Lee, Design solutions to minimize iron core loss in synchronous reluctance motor using Preisach model and FEM, IEEE Trans. Magn. 38 (2002) 3276–3278.
[21] J.G. Zhu, S.Y. Hui, W.S. Ramsden, Discrete modeling of magnetic cores including hysteresis eddy current and anomalous losses, IEE Proc. A 140 (1993) 317–322.
[22] S.Y.R. Hui, J. Zhu, Magnetic hysteresis modeling and simulation using the Preisach theory and TLM technique, in: Power Electronics Specialists Conference, vol. 2, Taibei, Taiwan, 1994, pp. 837–842.
[23] D.X. Xie, W.M. Zhang, B.D. Bai, et al., Finite element analysis of permanent magnet assembly with high field strength using Preisach theory, IEEE Trans. Magn. 43 (2007) 1393–1396.
[24] H. Mitsuo, M. Takeshi, H. Masashi, Three-dimensional finite element eddy current analysis by using high-order vector elements, Electr. Eng. Jpn. 147 (2004) 60–67.
[25] D.X. Xie, O.A. Mohammed, G.F. Ule, C.S. Koh, T–Ω finite element analysis of 3D nonlinear transient eddy current problems, Adv. Comput. Des. Tech. Appl. Electromagn. Syst. (1995) 211–214.
[26] O. Biro, K. Preis, On the use of the magnetic vector potential in the finite element analysis of 3-D eddy current, IEEE Trans. Magn. 25 (1989) 3145–3159.
[27] O. Biro, K. Preis, An edge finite element eddy current formulation using a reduced magnetic and a current vector potential, IEEE Trans. Magn. 36 (2000) 3128–3130.
[28] J.S. Weljj, Calculation of eddy currents in terms of H on hexahedra, IEEE Trans. Magn. 21 (1985) 2239–2241.
[29] O.A. Mohammed, F.G. Uler, A state space approach and formulation for the solution of nonlinear 3-D transient eddy current problems, IEEE Trans. Magn. 28 (1992) 1111–1114.
[30] J. Jin, The Finite Element Method in Electromagnetics, Wiley-IEEE Press, New York, 2002.